npj Urban Sustainability

https://doi.org/10.1038/s42949-026-00411-3

Article in Press

Underestimated mortality risks from compound urban heat and air pollution islands in Global North cities

Received: 30 October 2025

Accepted: 15 May 2026

Cite this article as: Lin, Y., Zhang, H., Chakraborty, T. *et al.* Underestimated mortality risks from compound urban heat and air pollution islands in Global North cities. *npj Urban Sustain* (2026). https://doi.org/10.1038/s42949-026-00411-3

Yinyi Lin, Hongsheng Zhang, TC Chakraborty, Shan Wei, Yanjia Cao, Jing Wei, Peng Gong & Yuyu Zhou

Underestimated Mortality Risks from Compound Urban Heat and Air Pollution Islands in Global North Cities

Yinyi Lin[1], Hongsheng Zhang*[1,2], TC Chakraborty[3], Shan Wei[1], Yanjia Cao[1], Jing Wei[4], Peng Gong[1,2], Yuyu Zhou*[1,2]

[1]The Department of Geography, The University of Hong Kong, Hong Kong SAR, China

[2]Institute for Climate and Carbon Neutrality, The University of Hong Kong, Hong Kong SAR, China

[3]Atmospheric, Climate, & Earth Sciences Division, Pacific Northwest National Laboratory, WA, USA

[4]MEEKL-AERM, College of Environmental Sciences and Engineering, Institute of Tibetan Plateau, and Center for Environment and Health, Peking University, Beijing, China

* Corresponding Authors: Hongsheng Zhang (zhanghs@hku.hk); Yuyu Zhou (yuyuzhou@hku.hk)

Abstract

Exposure to extreme heat and air pollution brings significant risks to human health and well-being. Urbanization can increase local exposure to high temperature and air pollution through the urban heat and air pollution islands (UHI and UPI), respectively. Previous studies have mainly focused on heat or air pollution separately, with limited consideration of the combined impacts on health in global cities. In this study, we investigate the daily 1km compound patterns of UHI and UPI using the satellite-based air temperature and $PM_{2.5}$ datasets and their combined impacts on mortality among 327 global cities from 2003 to 2020 with the exposure–response functions and structural equation modelling. Global South cities experienced 1.4 times higher compound frequency of UHI and UPI compared to Global North cities, whereas Global North exhibited greater compound intensity. Global South cities experienced 625 times, well over two orders of magnitude, higher compound exposure to extreme heat and air pollution. By contrast, Global North cities showed the higher relative risks to high temperature-related mortality linked to elevated compound frequency/intensity of UHI and UPI levels. These findings underscore the urgent need for region-specific urban heat mitigation strategies, i.e., reducing absolute background exposures in the Global South and managing relative UHI and UPI amplification in the Global North, as tailored interventions that are critical for lowering mortality risks and fostering healthier, more equitable cities worldwide.

Keywords: Urban heat island, urban pollution island, compound risk, air pollution, human health, urbanization, Global South

Introduction

Increasing exposure to environmental extremes from global warming and air pollution significantly enhances risks to human health and well-being[1-3]. Urbanization modifies local temperature and air pollution, leading to urban heat islands (UHI)[4] and urban air pollution islands (UPI)[5], respectively (Supplementary Fig. 1). These added urbanization-induced environmental stressors impact a disproportionate number of people due to the high population density of urban agglomerations[6,7]. Although extreme heat and air pollution individually contribute to negative health impacts, the combined risks of heat and air pollution, as well as the role of urbanization in exacerbating these risks, are still poorly understood in cities worldwide[8], particularly in both the Global North and Global South, where contrasting socioeconomic and physical infrastructures result in varied health outcomes[9]. Such information is vital for formulating optimum strategies for sustainable urban development in a warming and rapidly urbanizing planet.

Compound hazards often increase health and well-being risks in urban areas[10]. Firstly, temperature will have impact on the formation of air pollution. Heat waves and drought can exacerbate the air pollution burden[11]. Near-surface meteorological variables that are frequently modified by urbanization, such as temperature, humidity, and wind speed[12], can influence the formation of particulate matter, which are major contributors to air pollution[13]. The compound effects of heat and air pollution can lead to more severe respiratory and cardiovascular issues for individuals exposed to polluted air during heat waves[14]. Secondly, global scale studies of these compound events are limited by their focus on single extreme heat factors, their regional/local specificity, and the lack of high-resolution environmental and health data across diverse urban areas. Most existing global studies have primarily focused on the impacts of extreme heat alone[1,15], the compound effects of extreme temperatures and air pollution on health are often underexplored[8]. Local and regional studies have examined the health impacts of these combined stressors[16-18]. Heat-air pollution interactions changed the patterns of allergy and asthma and all-cause mortality in European cities[8,16]. Maternal exposure to air pollutants with higher temperature was associated with higher preterm birth risks in China[17]. Research in California has found that the combined exposure to extreme temperatures and the fine particulate matter with a diameter of less than 2.5 microns ($PM_{2.5}$) is associated with a higher risk of cardiovascular and respiratory mortality than the sum of their individual effects[18]. However, comparable analyses at the global scale are not yet widely available. Moreover, most studies have relied on coarse resolution environmental data (e.g., 0.1 degree resolution temperature and air pollution data)[1,8,19] or sparse observations from stations[2], which is insufficient for capturing the local-scale variations critical for urban health assessments. Third, the compound effects of extreme heat and air pollution disproportionately affect vulnerable populations. Studies in the United States have consistently found that marginalized communities, including low-income neighborhoods and people of color, are more impacted by both extreme heat and air pollution in urban areas[20-22]. These compound effects can further exacerbate existing health disparities and socioeconomic inequalities. While previous studies have examined the health impacts of extreme heat and air pollution individually, and in some cases jointly at local level, there remains a critical need for a systematic, global-scale analysis of their compound effects, particularly to understand and address disparities in health risks across regions.

Urbanization locally intensifies the temperature and air pollution compared to the background climate, forming the UHI and UPI, which both pose risks to the residents' health. Different urban forms and urbanization trends will lead to different UHI and UPI interaction patterns[23]. Previous study indicates that urbanization increases the daytime and nighttime heat-related mortality risk in cities[15,24]. It is found that the mortality risks are higher in high UHI and extreme heat scenarios in Hong Kong[25] and Toyko[26]. UHI can bring dual impacts on mortality in 3,000 cities worldwide[27]. Besides, urbanization can increase the $PM_{2.5}$ concentration, increasing vulnerability to air pollution in dense urban areas[28]. Research in Moscow indicated that the UHI and UPI may interact together and brought higher association between the high temperature and mortality through the increasing precipitation and road dust[29]. The canopy UHI can be measured by the difference of urban and rural temperature, which demonstrates close relationship with human comfort, energy consumption and health[30]. While in-situ measurements provide high accuracy measurement for UHI/UPI at individual sites (e.g., Berlin[31] and Birmingham[32]), they lack spatial representativeness across heterogeneous urban landscapes. Regional modeling studies from reanalysis data/numerical modelling have advanced our understanding but remain limited by computational tradeoffs between resolution and domain size[30,33]. Satellite-derived products offer global coverage, yet prior efforts have either focused on singular phenomena (UHI or UPI)[5,27], or used land surface temperature proxies in dense urban cores[34,35]. Consequently, a critical gap persists in high spatial (1 km) and temporal (daily) resolution, globally consistent quantification of compound UHI and

UPI patterns, particularly across the Global South and Global North cities where rapidly urbanizing patterns and spatial heterogeneity are different. This complex relationship between urbanization and health risks needs to be better understood to balance urbanization development with heat mitigation measures for healthy and sustainable cities.

To address these knowledge gaps, we examined global compound frequency and intensity of UHI and UPI, population exposure to compound heat and air pollution, and its association with health impacts. In this study, we aim to address three research questions: (1) What is the spatiotemporal pattern of compound frequency/intensity of UHI and UPI in global cities? (2) What is the compound exposure and mortality risk from heat and air pollution? and (3) How does urbanization influence the frequency and intensity of compound UHI and UPI, and what are its impacts on compound exposure and heat-related mortality? We followed the "Driving Forces – Pressures – State – Exposure – Effect – Action" (DPSEEA) framework[14,36], a widely used approach in environmental health research for understanding how societal and environmental factors influence health outcomes. In this study, urbanization is considered as the driving force; the UHI and UPI represent the pressures related to human activities; the state refers to the occurrence of extreme heat and air pollution; and population exposure to these extremes is analyzed as the exposure component. We then assess the associated compound health impacts (effect), and explore urban greening as a potential mitigating action. Specifically, the $PM_{2.5}$ is used as an indicator for urban air pollution for its widely recognized health impacts[37] and the spatial coverage of high-resolution datasets across urban agglomerations[38]. We first calculated the compound frequency, intensity and trend of UHI and $PM_{2.5}$-based UPI for 327 global cities from 2003 to 2020 at 1km spatial resolution. The period from 2003 to 2020 were selected based on the availability of consistent, high-resolution satellite-derived and ground-calibrated environmental datasets, including daily near-surface air temperature and $PM_{2.5}$ concentrations at a global scale. UHI intensity was calculated using daily mean air temperature, derived from both daytime and nighttime air temperature to represent the overall urban thermal background[27]. To evaluate the compound effects of UHI and UPI, we defined two key metrics, compound frequency (the number of days per year when both UHI and UPI co-occur) and compound intensity (the combined intensity of these two phenomena). Then, we analyzed the population exposure to compound heat and air pollution within cities at 1 km resolution. Next, the compound frequency and intensity of UHI and UPI's impact on the cumulative relative risk (RR) of high temperature was analyzed using exposure–response modeling[39-41]. The daytime maximum air temperature was considered for the high temperature related mortality risk analysis. Finally, the potential impacts of urbanization and urban greening mitigation measures were analyzed using structural equation modeling[42], which can explore the direct and indirect relationships among urbanization, compound UHI and UPI patterns, and environmental stressors.

Results

Spatial patterns and temporal trends of compound frequency and intensity of UHI and UPI

Global South cities had higher compound frequency of UHI and UPI but slightly lower intensity compared with Global North cities. Cities in the Global South experienced a greater compound frequency of UHI and UPI ($P<0.05$), with approximately 94 days per year from 2003 to 2020 (Fig. 1b). Cities in the Global North experienced a lower compound frequency (average 69 days per year). Cities in West and Southeast Asia had higher frequency than the other regions (Fig. 1a and Supplementary Fig. 2) while cities in southern Europe had higher intensity (Supplementary Fig. 3). Generally, cities in Global North had slightly higher CUHPI (ranging from 0 to 1) with an average of 0.856 compared with 0.849 in Global South ($P<0.05$). The CUHPI indicated the compound intensity of UHI and UPI. Global North cities had a higher UHI intensity with an average of 0.75˚C, while the Global South cities had a lower UHI intensity of 0.51˚C. Unlike the UHI, the UPI showed higher intensity and frequency in Global South cities (Supplementary Fig. 5&6). Global South cities had a higher UPI intensity of 3.46 $\mu g/m^3$ compared with the Global North cities, with a lower UPI intensity of 1.46 $\mu g/m^3$. Usually, cities in high-income countries, particularly those located in Oceania and parts of Asia or in arid climates, generally exhibited higher UHI intensity, whereas cities in low-income countries, mainly in Africa and South America or in arid and continental climates, tended to show higher UPI intensity (Supplementary Figs. 11–13). Cities in the Global South showed a trade-off relationship between UHI and UPI in winter and summer but only showed a large difference in winter in the Global North (Supplementary Fig. 9). There were some cities with compound frequency of UHI and UPI more than 310 days per year, including Karaj, Tehran, Tabriz in Iran, Bayrut (Beirut) in Lebanon, Ciudad de México (Mexico City) in Mexico, Manila, Antipolo, Bacoor, Dasmarinas and Imus in Philippines, and Tashkent in Uzbekistan (Fig. 1e). The top five urban agglomerations with the highest CUHPI were Karaj and

Tehran in Iran, Bayrut (Beirut) in Lebanon, Nice-Cannes in France, and Tokyo in Japan (Supplementary Fig. 10).

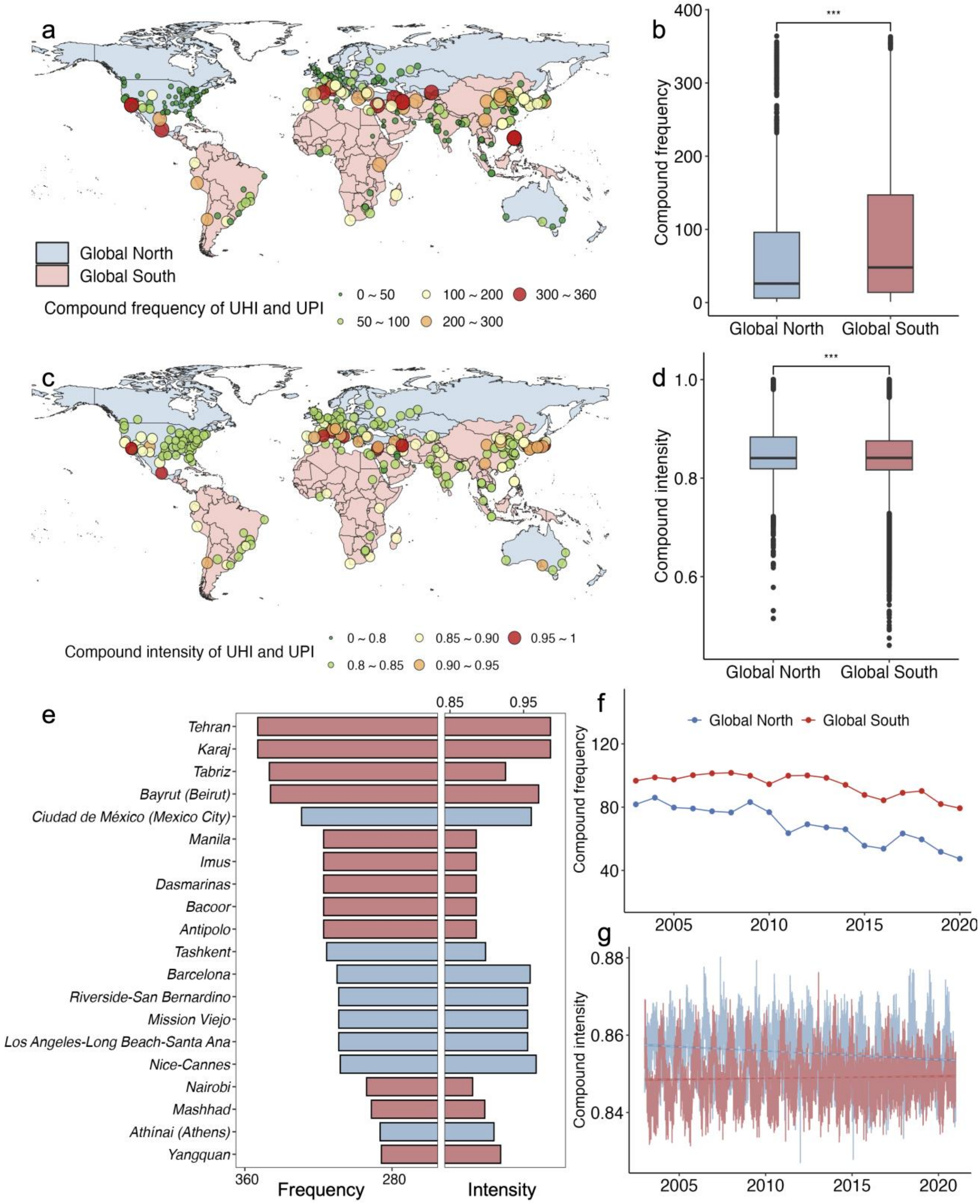

Fig. 1 | Compound frequency and intensity of UHI and UPI in 327 cities from 2003 to 2020. a, Annual mean compound frequency of UHI and UPI (number of days/year) for global cities from 2003 to 2020. **b**, Summary of compound frequency of UHI and UPI of Global North and Global South cities from 2003 to 2020. **c**, The mean compound intensity of UHI and UPI for global cities from 2003 to 2020. **d**, Summary of compound intensity of UHI and UPI of Global North and Global South cities from 2003 to 2020. **e**, The top 20 cities with the highest compound frequency of UHI and UPI and their associated compound intensity of UHI and UPI. **f**, Time series compound frequency of UHI and UPI for Global South and Global North cities from 2003 to 2020. **g**, Time series compound intensity of UHI and UPI for Global South and Global North cities from 2003 to 2020. Pairwise T-tests were conducted to determine the significance level between the Global North and South cities. '***' indicates significant differences at the 0.001 levels.

Global cities experienced a decreasing trend of both compound frequency and intensity of UHI and UPI (Fig. 1f&g). Among 327 cities, 54 cities showed a significant increasing trend ($p<0.05$) of compound frequency of UHI and UPI, while 130 cities showed a significant decreasing trend ($p<0.05$) (Supplementary Fig. 4). Global North cities showed a higher decreasing trend of compound frequency comparing with Global South cities ($p<0.05$). There were 160 cities showing a decreasing trend of compound intensity of UHI and UPI and 133 cities showing an increasing trend ($p<0.05$). Global North cities showed a decreasing trend of compound intensity while the Global South cities showed an increasing trend. Overall, the UHI frequency and intensity showed an increasing trend, while both UPI frequency and intensity showed a decreasing trend (Supplementary Fig. 7&8). Specifically, 188 cities showed a significant increasing trend ($p<0.05$), while 92 cities showed a significant decreasing trend ($p<0.05$) of UHI intensity. 115 cities showed an increasing trend ($p<0.05$) of UPI intensity, while 169 cities showed a decreasing trend ($p<0.05$). Both the compound frequency and intensity of UHI and UPI have declined during the COVID-19 period (Fig. 1f&g).

Global population's compound exposure to extreme heat and air pollution

Cities in the Global South experienced compound exposure to heat and air pollution (i.e., $PM_{2.5}$ in this study) that was approximately 625 times greater than in cities of the Global North (Fig. 2a&b). Generally, the global average population's exposure to extreme heat has been intensifying, while the population's exposure to high air pollution has reduced, especially since 2013 (Fig. 2d). The compound exposure to extreme heat and air pollution remained stable in this period and has seen a slight decline after 2018 (Fig. 2c). Global South cities are more at risk since they have higher extreme heat exposure and $PM_{2.5}$ exposure, and a higher density of population, which results in higher compound exposure to extreme heat and air pollution with an average exposure of 25 million person-days per year per city compared with 0.04 million in Global North, approximately 625 times higher of the Global North. Delhi (India), Bhiwandi (India), Mumbai (India), Lahore (Pakistan), and Al-Khartum (Sudan) were the top five cities with the highest compound exposure to heat and air pollution. There were approximately 4.88 million person-days per year in a city exposed to compound extreme heat and air pollution and facing compound UHI and UPI situations (Fig. 2e).

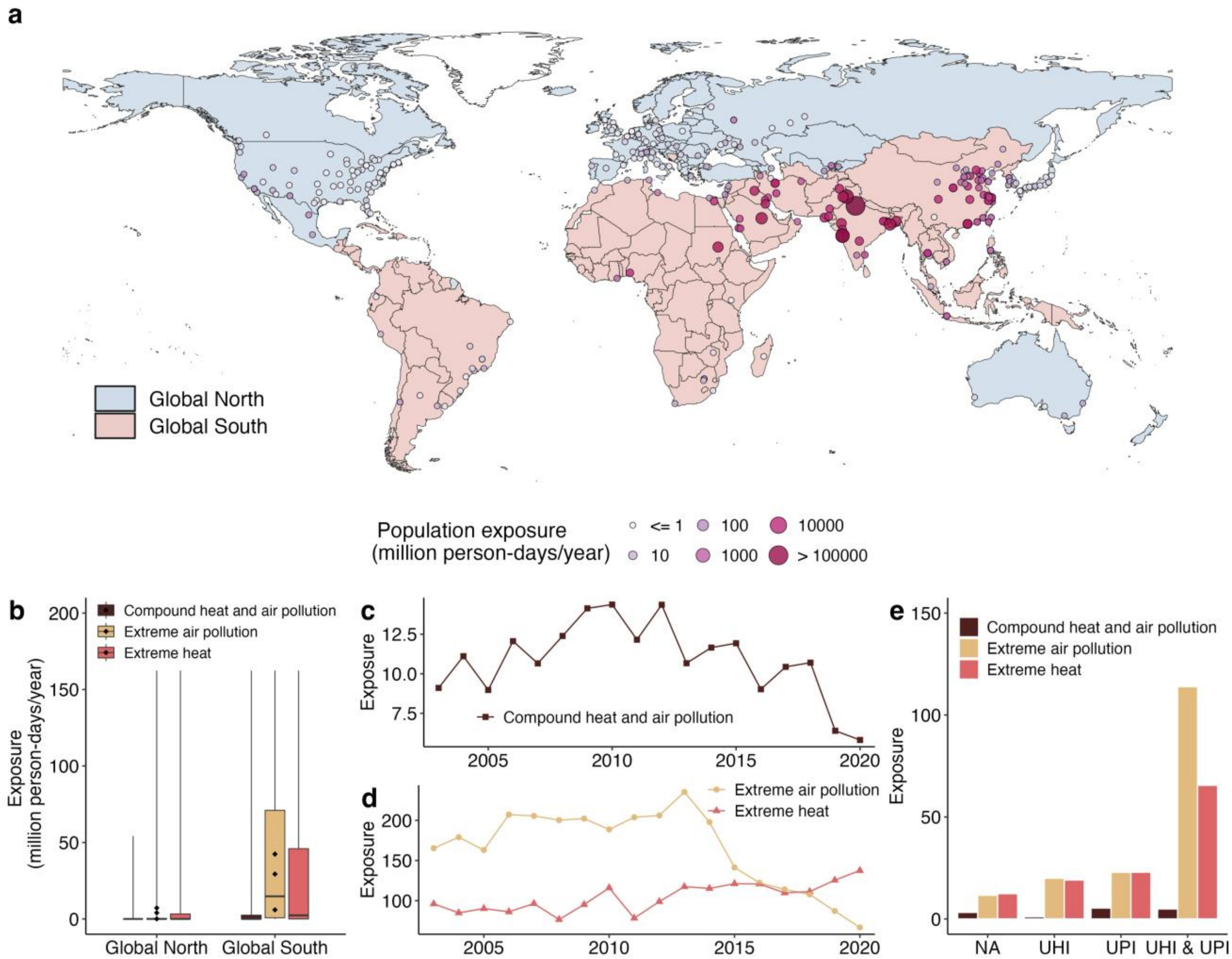

Fig. 2 | Compound exposure to extreme heat and air pollution in global cities. a, Averaged compound exposure to heat and air pollution **(**$PM_{2.5}$) from 2003 to 2020, the threshold of daily extreme heat was 35 degrees and the threshold of daily extreme $PM_{2.5}$ was 75 ug/m^3. **b**, Averaged exposure (million person-days/year) to heat, $PM_{2.5}$ and compound exposure of cities in Global North and Global South from 2003 to 2020. **c**, Time series annual compound exposure (million person-days/year) to extreme heat and air pollution of cities from 2003 to 2020. **d**, Time series annual exposure (million person-days/year) to extreme heat and air pollution of cities from 2003 to 2020. **e**, Averaged exposure (million person-days/year) to heat, $PM_{2.5}$, and compound exposure of cities with UHI, UPI, both UHI & UPI and non UHI & UPI (NA) from 2003 to 2020.

Health mortality risks associated with high temperature in cities with compound intensity and frequency of UHI and UPI

Cities with higher compound frequency or intensity of UHI or UPI levels generally tended to have higher cumulative risk (RR) for mortality rate related to high temperature, especially for the elderly groups (Fig. 3a, b & e). The cumulative RR was higher in cities with higher compound frequency of UHI and UPI (79 days per year) (Cumulative RR=1.020, 95% CI: 1.008-1.031), comparing with lower compound frequency levels (5 days per year) (Cumulative RR=1.009, 95% CI: 0.996- 1.022). The cumulative RR is also higher in the higher compound intensity of UHI and UPI levels (Cumulative RR=1.019, 95% CI: 1.009-1.030). Specifically, the cumulative RR was higher in the cities with higher UHI level (0.8 $^{\circ}C$) (Cumulative RR=1.017, 95% CI: 1.006-1.028) comparing with the lower UHI level (0.3 $^{\circ}C$) (Cumulative RR=1.010, 95% CI: 0.998-1.023) (Supplementary Fig. 16). The cumulative RR was also higher in higher UPI levels with cumulative RR of 1.018 (95% CI: 1.006-1.028). The female group (Fig. 3d) and the elderly (age higher than 75 years old) showed a higher cumulative RR (Fig. 3e). The cities in Global South showed a different pattern, since many of these cities located in the tropical climate, which have already been exposed to background heat extreme environment, making the UHI/UPI is not a dominant issue in these cases.

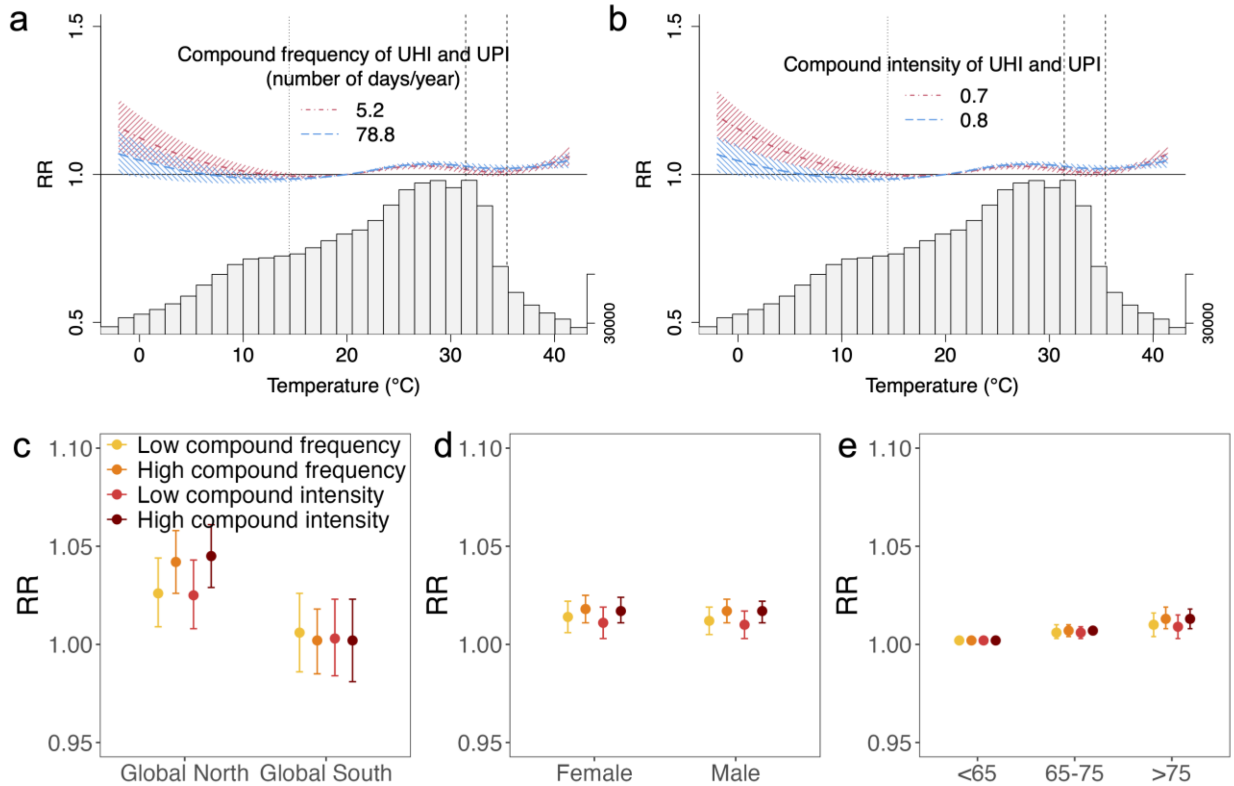

Fig. 3 | Cumulative relative risk (RR) of cities in high (75th percentile) and low (25th percentile) compound intensity and frequency of UHI and UPI levels and different groups. a, RR in high and low compound frequency of UHI and UPI levels. **b**, RR in high and low compound intensity of UHI and UPI levels. **c**, RR of cities in Global North and in Global South with different compound frequency of UHI and UPI, and compound intensity of UHI and UPI levels. **d**, RR of different sex groups in global cities with different compound frequency of UHI and UPI, and compound intensity of UHI and UPI levels. **e**, RR of different age groups in global cities with different compound frequency of UHI and UPI, and compound intensity of UHI and UPI levels. The vertical lines denote the percentile of minimum mortality temperature (dotted) and the 90th and 99th percentiles of the temperature distribution (dashed).

Effects of urbanization, compound factors, and greening, on mortality and exposure

Cities in the Global South exhibited stronger compound effects of extreme temperature and $PM_{2.5}$ on both compound exposure and mortality, whereas cities in the Global North showed greater impacts from compound patterns of UHI and UPI. Using the structural equation model, we tested the interactive associations of urbanization, compound frequency of UHI and UPI, compound intensity of UHI and UPI, temperature, and $PM_{2.5}$'s impact on mortality rate and exposure (Fig. 4). Temperature had a positive effect (direct impact, 0.24, 95% Confidence Interval (CI): 0.19-0.30) on the high temperature-related mortality rate, which means a unit increase in temperature corresponds to a 0.24 unit increase in mortality rate (Fig. 4d). Similarly, temperature also showed a positive effect (0.33, 95% CI: 0.31-0.35) on the compound exposure to extreme heat and air pollution (Fig. 4a). A significant positive partial correlation can also be observed between $PM_{2.5}$ and mortality rate (0.62, 95% CI: 0.54-0.71) (Fig. 4d) and between $PM_{2.5}$ and exposure (0.54, 95% CI: 0.52-0.56) (Fig. 4a). Thurs, the total impact of temperature on mortality rate (total effect) was further mediated via the $PM_{2.5}$ pathway (indirect). The total effect of temperature is obtained by adding the direct effect of temperature on mortality rate and the indirect effect via PM2.5. The total effect of temperature on exposure and mortality is higher in Global South than Global North in both SEM (Fig. 5a & Table S5&6) and multilevel interaction model (Fig. 4 b&e). In contrast, the total effects of compound intensity and frequency on mortality and exposure are higher in the Global North (Fig. 5b, Fig. 4 c&f), with compound intensity showing highest positive total effect on compound exposure (0.37, 95%:0.30-0.44). Notably, in the Global South, compound intensity and frequency exhibit a negative association with mortality and exposure. Urbanization also indirectly enhanced the mortality rate due to the positive correlation with heat (0.57, 95% CI: 0.52-0.61) and $PM_{2.5}$ (0.25, 95% CI: 0.18-0.32) (Fig. 4d). Urban greening showed a negative correlation with $PM_{2.5}$ (-0.28, 95% CI: (-0.32)-(-0.23)) and temperature (-0.16, 95% CI: (-0.20)-(-0.11)), which can potentially and partially mitigate the total negative impacts of $PM_{2.5}$ and local urban heat.

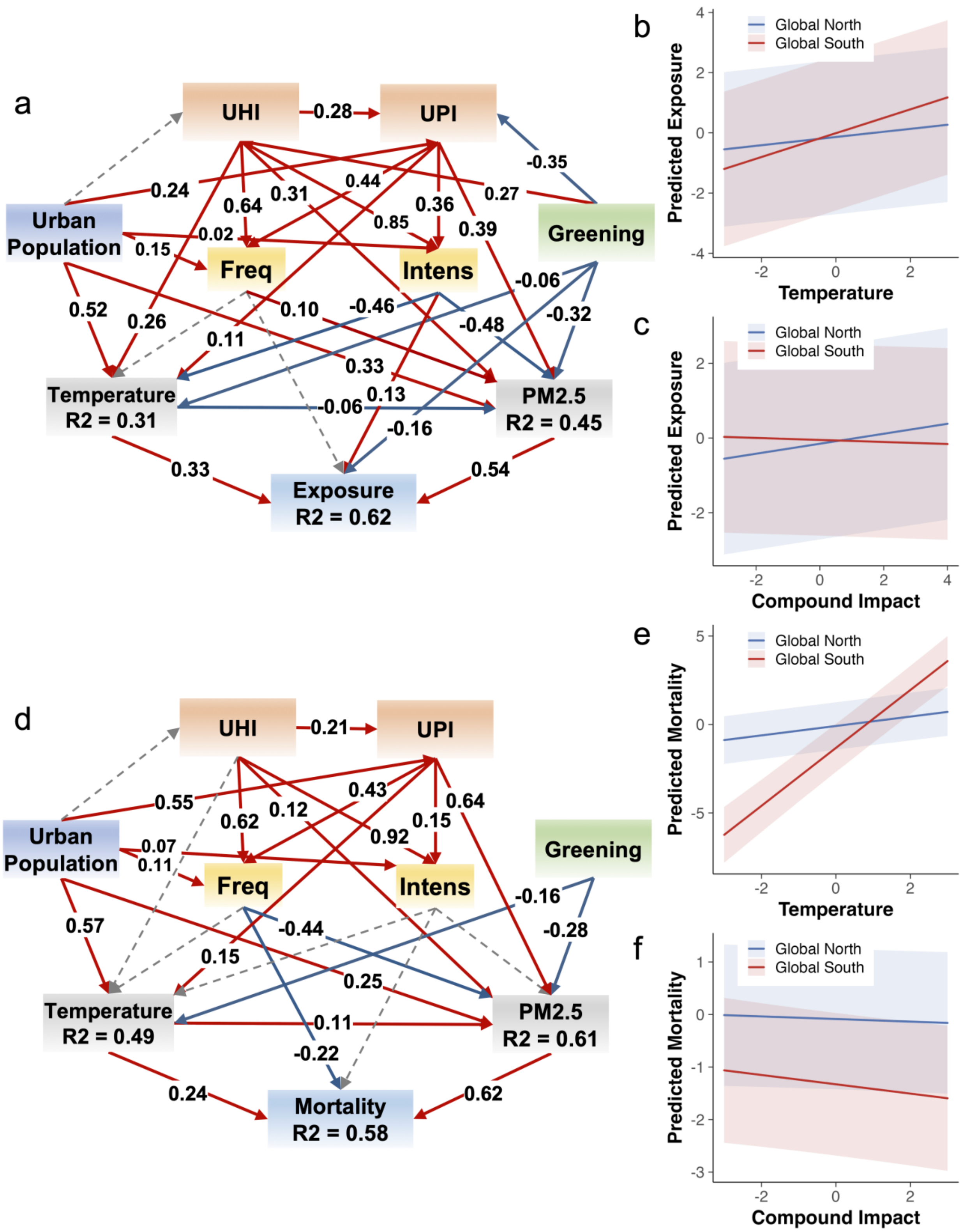

Fig. 4 | The structural equation model of the correlation of annual urban population, compound frequency of UHI and UPI, compound intensity of UHI and UPI, $PM_{2.5}$, temperature, greening and exposure/mortality at city level from 2003 to 2019. **a**, Correlation among the urban population, compound frequency of UHI and UPI, compound intensity of UHI and UPI, temperature, $PM_{2.5}$, greening and exposure (N=4173) using structural equation model (SEM). **b**, Multilevel regression between temperature and compound exposure. **c**, Multilevel regression between compound impact (compound intensity and compound frequency) and compound exposure. **d**, Correlation among the urban population, compound frequency of UHI and UPI, compound intensity of UHI and UPI, temperature, $PM_{2.5}$, greening and mortality rate (N=936) using the SEM. **e**, Multilevel regression between temperature and mortality rate. **f**, Multilevel regression between compound impact (compound intensity and compound frequency) and mortality rate. Freq indicates the compound frequency of UHI and UPI and Intens indicates the compound intensity of UHI and UPI. Urbanization is indicated by the mean urban population density within the urban areas. Urban greening is indicated by mean NDVI within the urban areas. The red arrows show the positive effect while the blue arrows show the negative effect with significant level P<0.01. The dash grey arrows indicate the insignificant effect. The values on the arrow indicate standardized coefficients and statistical significances of the endogenous variables.

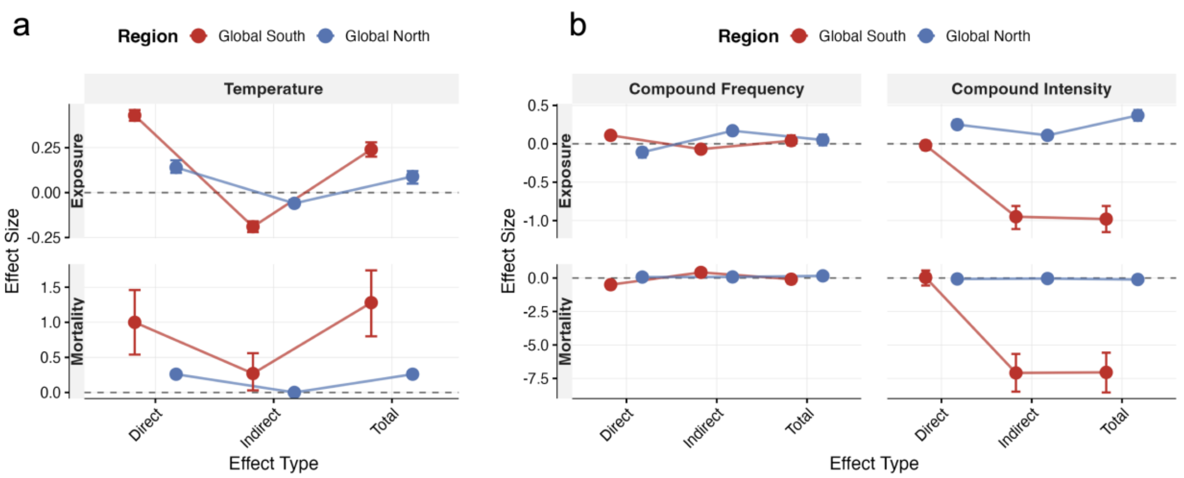

Fig. 5 | Direct, indirect and total effects of temperature and compound patterns of UHI and UPI on mortality rate/exposure in Global South and Global North cities. a. The direct, indirect and total effects of temperature. b, The direct, indirect, and total effects of compound frequency of UHI and UPI, and compound intensity of UHI and UPI.

Discussion

Compound patterns of UHI and UPI and compound exposure to extreme heat and air pollution lead to higher risks to human health, while disparities exist by different spatial regions and population groups, which exacerbates impacts of urbanization. With the higher intensity and frequency of climate extremes, the interaction between heat exposure and other environmental stressors will become more prevalent. It is essential to evaluate the combined impacts of these factors comprehensively. Our results reveal a contrast between the Global South and Global North in the drivers of compound heat and air pollution risks. In the Global South, absolute background levels of temperature and $PM_{2.5}$, together with large population size and high social vulnerability, dominate health outcomes. Cities such as Sindh, Punjab, and Pernambuco face persistently extreme baseline conditions that exceed physiological and regulatory thresholds, resulting in high mortality despite modest UHI and UPI intensity. By contrast, in the Global North, relative urban increments, i.e., compound frequency and intensity of UHI and UPI, play a larger role in driving temperature related mortality, as they often push otherwise moderate background conditions beyond critical health thresholds. Urbanization is usually related to dramatic urban expansion, which enhances the difference in temperature and air pollution between urban areas and their surroundings. Urban residents, in this case, face both intensifying heat and air pollution stress. While studies indicate that global air pollution is reducing[43], urbanization-related UPI magnifies the local air pollution exposure, further compounded by increased population migration to cities across scales. In addition, climate change, which intensifies extreme temperatures, has worsened this situation[44]. With elderly populations being more vulnerable than other groups and the world population gradually aging, the compound heat and air pollution stress have disproportionate impacts[45]. It underscores the need for region specific adaptation strategies, targeting absolute exposure reductions in the Global South and urban amplification mitigation in the Global North.

Our results demonstrate both the compound frequency and compound intensity showed a decreasing trend, with increasing trends of UHI and decreasing trends of UPI. The decreasing trend of UPI can be attributed to air pollution clean-up efforts. In China, the national air quality action plans has led to measurable improvements in air quality since 2013[46], which provide a useful model for other rapidly urbanizing regions. However, cities in parts of South Asia, particularly India, remain highly vulnerable to compound heat and pollution stress due to persistent high emissions, rapid urban growth, and limited mitigation infrastructure[47] (Supplementary Fig. 14). A noticeable decrease in UPI levels in 2020 across many cities has been observed, which aligns with global patterns of reduced economic activity during the initial phases of the COVID-19 pandemic (Supplementary Fig. 22). This temporary decline is consistent with prior research showing sharp reductions in transportation and industrial emissions during lockdowns[48,49]. However, UPI levels began to rebound in some cities in late 2020 and into 2021 as restrictions eased and activity resumed, indicating that the decrease was not sustained in many locations. Due to our study period ending in 2020, we are unable to fully capture the extent of recovery in subsequent years. Improved urban greenness exposure can also be observed in recent decades[50]. Greening, on one hand, can reduce local temperature, provide shading, and increase evapotranspiration, reducing the negative impacts of urban heat islands in many situations[51]. On the other hand, the $PM_{2.5}$ can be deposited on vegetation, thereby purifying the air. Our structural equation modeling results indicate that urban greening is significantly associated with lower $PM_{2.5}$ levels, suggesting that nature-based solutions can contribute meaningfully to pollution reduction. A recent study indicates that Global South and Global North cities experience disproportionate inequalities of urban green spaces[52], including parks, green roofs, and vegetated sidewalks. This notable disparity in the distribution of urban green infrastructure between cities in the Global South and Global North, would lead to significant cooling, and thus inequalities in health impact[52]. Our analysis suggests that urban greening, as proxied by NDVI, may play a mitigating role in high temperature related mortality. The Climate and Clean Air Coalition (CCAC) from UNEP has pinpointed 25 clean air measures aimed at alleviating the health impacts of both climate change and air pollution. There is a pressing need to incorporate multidisciplinary sectors, such as urban planning, green construction, energy use, health care and air pollution control, into policy considerations to mitigate the combined impacts of urban heat and air pollution.

Cities in the Global South with lower UHI intensity also exhibited higher compound exposure of extreme heat and air pollution. Many of these cities are located in tropical climates and tend to have more sprawling urban forms and in many cases, limited infrastructure and public service coverage[53]. These structural and spatial factors may contribute to increased vulnerability, even in the presence of moderate UHI intensity. While UHI contributes to elevated urban temperatures, it is ultimately absolute temperature, not the urban and rural temperature differential that drives health risk[54]. Therefore, effective urban climate adaptation should focus on reducing harmful temperature extremes overall, rather than only narrowing the UHI gap. We also note real-world examples of compound exposure events, such as the 2010 Moscow heatwave and wildfire smoke crisis, which led to a substantial increase in all-cause mortality[55]. As shown in Supplementary Fig. 23, elevated temperatures are evident throughout the July 6–August 18 period, while $PM_{2.5}$ levels peak in early August, consistent with the smoke event. Notably, we observe an increased UPI substantially during this event. Although our study does not explicitly distinguish wildfire smoke from other pollution sources, we observe episodic spikes in $PM_{2.5}$ and UPI intensity that correspond with known wildfire events, particularly in parts of western North America. These patterns suggest that wildfire smoke may be a growing driver of compound urban heat and pollution exposure**,** even in high-income countries where anthropogenic emissions have declined. In cities such as San Francisco, $PM_{2.5}$ levels occasionally exceed those of some Global South cities during wildfire seasons (Supplementary Fig. 24). It also highlights the applicability of our compound metrics in identifying and characterizing real-world hazard events.

Global North cities experienced a higher risk from relative impacts from compound UHI and UPI. Urbanization contributes to the development of UHI, while industrial and other anthropogenic activities in cities can result in the formation of UPI[31]. UHI demonstrates a negative relationship with UPI (ρ=-0.26, $P<0.001$) (Supplementary Fig. 17), suggesting an inverse spatial or temporal relationship between urban heat and pollution islands. Elevated temperatures can increase the height of the urban boundary layer, enhancing atmospheric mixing and thereby facilitating the vertical dilution of air pollutants[56]. The negative relationship also reveals the disparity of relatively high UHI of cities in Global North and relatively high UPI of cities in Global South. Specifically, we find a negative relationship between UHI and ambient temperature, which reflects the commonly observed dampening of UHI intensity during extremely hot days, when rural areas also experience substantial warming, reducing the urban and rural temperature gradient[57]. In contrast, UPI shows no significant relationship with temperature, suggesting that short-term thermal conditions do not consistently modulate $PM_{2.5}$ concentration differences between urban and rural areas. However, UPI is positively associated with $PM_{2.5}$ levels, validating its role as an indicator of relative pollution accumulation in cities. Specifically, the compound frequency of UHI and UPI will intensify the urban temperature (ρ=0.13, $P<0.001$), which may potentially increase the risks of mortality. We should note here that the UHI is not always a negative environmental stressor. For instance, UHI provides warmth in winter for high-latitude cities[27]. Wang et al. (2025) found that the UHI effect can reduce cold-related mortality while increase heat-related mortality, with the reduction in cold-related deaths often outweighing the increase in heat-related impacts. Our findings similarly reveal the dual and often imbalanced health implications of UHI, as well as the compound effects of UHI and UPI. We also observed that relative risk (RR) increases more steeply at lower temperature ranges in some cities, reflecting the elevated cold-related mortality risks previously identified in multi-city epidemiological studies[40,41,58]. This asymmetry highlights the importance of considering both ends of the thermal exposure spectrum and tailoring mitigation strategies to regional vulnerabilities. This complex interplay between urbanization, pollution, and heat highlights the need for comprehensive strategies to address the relative heat and air pollution impacts in Global North cities.

In future scenarios, the urbanization is projected to accelerate, particularly under fossil-fueled development scenarios, and urban expansion is likely to intensify local UHI and potentially cause regional warming[59]. As urbanization continues, the escalating number of urban dwellers in the Global South will confront significantly higher risks of compound impacts, as indicated by our population-weighted exposure estimations. Although overall pollution levels are anticipated to decrease in the coming decades, the UPI may not experience the same degree of reduction if urban anthropogenic activities and populations continue to grow. In addition, the rising intensity and frequency of heat waves associated with climate change, will further contribute to air pollution caused by wildfires in the warming scenario[60]. Consequently, we foresee an increase in population exposure to compound risks due to UHI and UPI, particularly in the Global South, while most Global North countries lack replacement fertility rates. Additionally, with the global population aging and becoming increasingly urbanized, vulnerability to heat is expected to rise further due to climate change, UHI[61], and the combined effects of UHI and UPI.

This study analyzed the combined effects of extreme heat and air pollution on heat-related mortality. However, we should note that urban heat may also contribute to pollution-related mortality. A key limitation of our analysis is the use of globally derived air temperature data that, while validated, may still carry uncertainties due to their statistical dependence on land surface temperature (LST) and available in-situ observations[62]. The air temperature dataset may remain indirectly influenced by LST and may partially inherit uncertainties associated with surface thermal heterogeneity, sensor overpass timing, and land-cover-dependent biases. LST is only an indirect proxy for human thermal environments, as thermal comfort and heat stress are primarily determined by near-surface air temperature together with humidity, radiation, and wind[63]. For the reduced station coverage in densely urbanized or data-sparse regions, spatial heterogeneity and vertical differences in urban heat signatures may not be fully captured, particularly for intra-urban

UHI variability. Besides, our UHI estimation is constrained by the spatial scale of available data. While we employ an urban and rural difference approach consistent with prior literature, more granular urban canopy modeling or high-density in situ networks would improve precision, especially in heterogeneous metropolitan regions. The frequency metrics reflects the occurrence of UHI conditions, while the intensity metric characterizes the magnitude of urban–rural temperature differences. The threshold of 0.5 $^{\circ}C$ is relatively conservative for the UHI frequency metric, sensitivity analyses using higher UHI thresholds (e.g., 1–2 $^{\circ}C$) yielded consistent Global South and Global North contrasts and temporal trends. The limitation of our UPI characterization is that it does not explicitly account for the directional dispersion of air pollution. In many cities, $PM_{2.5}$ forms elongated downwind plumes, influenced by prevailing winds and local topography[64]. These plumes may extend pollution exposure beyond the urban core, or conversely, shift peak pollution zones away from where UHI intensity is highest. As a result, our urban–rural contrast-based UPI estimates may underrepresent population exposure in some downwind areas or misalign with UHI hotspots, particularly in cities where emissions are strongly clustered or wind regimes are consistent. Incorporating wind direction and atmospheric transport models in future work would help address this spatial decoupling and improve compound exposure assessment. While UPI is not a direct measure of health risk, it reflects the differential pollution load between urban and rural areas, offering insight into the urban amplification of air pollution. However, during regional-scale pollution events, such as wildfire smoke, transboundary haze, or widespread industrial emissions, $PM_{2.5}$ concentrations in rural areas may approach or exceed those in cities, leading to a low UPI despite high absolute exposure and elevated health risk. This limitation underscores the importance of using absolute pollutant concentrations in parallel with UPI, which serves as a structural or contextual indicator rather than a direct exposure metric. The relatively limited use of UPI in the literature may reflect the complexity of spatial attribution in pollution dynamics, but we see value in introducing this concept to better characterize compound urban environmental burdens. In addition, nighttime UHI effects, which can exacerbate health impacts by preventing recovery during sleep, are not explicitly assessed in our daily-scale analysis. Future work should incorporate diurnal temperature cycles to better capture nocturnal heat retention and its implications for compound health stress. NDVI was used as a single proxy for urban greening, which was calculated using non-urban land cover within city boundaries to track changes in urban vegetation over time. While this method captures broad-scale greening, such as park expansion or reforestation in undeveloped areas, it may miss vegetation embedded within built-up urban zones**,** including street trees, courtyard gardens, or green roofs. The relationship between NDVI and air temperature reduction is complex and context-dependent, and we acknowledge that greening effects on air temperature and mortality cannot be fully captured through NDVI alone. Therefore, while NDVI has been widely used in large-scale environmental studies to estimate greenness[52], it may not fully represent the nuanced cooling and pollution-mitigating effects of green infrastructure. For a more detailed urban-scale analysis, high-resolution environmental data, such as 30 m surface temperature, land cover, and greening indices, can help better characterize the influence of urban morphology on local heat and pollution patterns. However, at this spatial scale, microclimatic factors such as shading, wind, and surface materials play a significant role[65], and human heat exposure is more accurately assessed using integrated thermal comfort metrics such as the Universal Thermal Climate Index (UTCI)[66], rather than air temperature alone. However, health data is only available at the provincial level at annual time intervals for global cities. Moreover, inter-urban variability in heat and pollution are difficult to get at sufficiently fine resolutions. We make a compromise between scale and availability of health and environmental data by considering urban agglomerations the units of analysis. The population exposure is estimated using a fixed threshold for extreme heat and/or pollution days. While this approach allows for standardization across cities, it does not account for spatial variation in climate adaptation. Prior work has shown that the health effects of temperature depend strongly on local norms, with heat-related mortality risks rising above city-specific thresholds such as the minimum mortality temperature (MMT)[41]. Incorporating such adaptive thresholds would improve the accuracy of exposure estimates, particularly for comparing mortality risk across diverse climates. Future research could refine this approach by integrating percentile-based thresholds or modelled MMTs based on historical climate and health records. Additionally, cities included in this study may be biased toward those with greater data availability, which often correlates with higher population density and more intense urban development. These characteristics can intensify both UHI and UPI effects[65], and as such, our results may overestimate compound exposure in comparison to smaller or less-developed urban areas. This limitation highlights the need for improved environmental and health data coverage in rapidly growing cities in the Global South. These limitations should be kept in mind when contextualizing the results of the study. With that being said, this analysis of the compound impacts of heat and air pollution on human health in cities is crucial for informing urban heat and adaptation strategies as we move towards a warmer and more urbanized future.

Methods

Urban and demographic data processing

Our urban region of interests was the global urban area boundary dataset from Natural Earth[67], and urban agglomerations information data (including name, city code, and country) were from the United Nations[68]. We initially considered the urban/metropolitan regions with a 2020 population higher than 500,000[69]. We further filtered the regions with area smaller than 500 square kilometers to ensure cities with small and irregular boundaries are removed and calculation uncertainties of UHI and UPI are minimized. A total of 327 cities/urban agglomerations, i.e., urban cluster were selected based on these criteria. Among them, 180 cities are located in the Global North, while 141 cities are in the Global South. The annual gridded population data were from LANDSCAN[70]. The urban population density were calculated using the zonal statistics of the mean urban population density within 1 km^2 population grid cells within the urban boundary.

Environmental data preprocessing

The environmental data included near-surface air temperature, $PM_{2.5}$, Normalized Difference Vegetation Index (NDVI), and land cover data. The daytime near-surface air temperature are from Zhang et al.[62,71] It measures the daily 2 m near-surface temperature data at 1km resolution using satellite observations and ground-station measurement obtained from a total of 103,156 weather stations. Cross validation with the daytime near-surface air temperature from the ground stations suggested an acceptable accuracy with root mean square errors ranging 1.20 to 2.44 °C across regions, which can capture the spatiotemporal patterns air temperature realistically, within acceptable ranges for large-scale epidemiological studies[27]. Validation against urban weather stations from National Climatic Data Center (NCDC) (Supplementary Fig. 18) in 327 cities showed a mean bias of 1.67°C for daily air temperature. While uncertainties remain, especially in densely built or data-sparse urban areas, this dataset offers a consistent and validated basis for multi-city comparison. The daily $PM_{2.5}$ data is from Wei et al.[38] The $PM_{2.5}$ concentration data are generated using machine learning and big data at 1 km resolution. Urban greening was obtained from the time series of the zonally averaged NDVI of non-urban land cover within each region. The NDVI was calculated from the difference between red and near-infrared surface reflectance from MYD09A1 v006 product[72], which is further aggregated into the yearly average at the pixel level. The annual land cover data were from MCD12Q1[73]. All the environmental data are at 1km resolution and all the geospatial analyses were done on the Google Earth Engine cloud computing platform[74].

Mortality data preprocessing

We collected the mortality data from the Global Burden of Diseases (GBD) from the Institute for Health Metrics and Evaluation (IHME)[75] in this study. It adopted a hierarchical list of risk factors. We considered the level three risk factors (attribute or exposure causally associated with increased incidence or prevalence of disease), i.e., the risk of high temperature of the non-optimal temperature under the environmental/occupational risk categories. The risk by high temperature, at all ages, and both sexes, and country-level/sub-national level of yearly death mortality count and rate data from 2000 to 2019 were considered. The metadata included the measure name (Deaths), location (country-level or subnational-level), sex (male, female and all sexes), age (<20 years, 20-54 years, 55-59 years, 60-64 years, 65-74 years, 75+ years, and all ages), and risk factors (high temperature), and year. The mortality rate and count data were used. We further converted the mortality count data to a logarithmic form for further processing. For age-based analysis, we divided the data into three age groups: those below 65 years, those between 65-74 years, and those older than 75 years.

Driving Forces–Pressures–State–Exposure–Effect–Action (DPSEEA) Framework

In this study, we adopt the Driving Forces–Pressures–State–Exposure–Effect–Action (DPSEEA) framework, widely used in environmental health research to trace the causal pathways from environmental drivers to health outcomes and heat mitigation strategies. Within this framework, urbanization serves as the driving force, shaping the demographic growth of cities. The pressures are represented by the UHI and UPI, which arise from anthropogenic emissions, land cover change, and built environment characteristics. The state reflects the physical environmental conditions, specifically the extreme heat and air pollution events. The exposure component captures the extent to which urban populations are exposed to these stressors, derived from high-resolution satellite datasets on air temperature and $PM_{2.5}$. The effect is quantified through estimated excess high temperature related mortality associated with different levels of compound frequency and intensity of UHI and UPI using established exposure–response functions. Finally, the action element is addressed by evaluating the potential of urban greening, measured via NDVI, as a mitigating factor capable of reducing population exposure and associated health risks using the SEM model. This structured approach allows us to systematically analyse the interconnected drivers, stressors, and outcomes of compound urban climate-health risks on a global scale.

Urban heat island intensity and trend

Urban heat islands (UHI) are defined as the air temperature difference between urban and rural areas. For each urban cluster, urban area was identified as the urban land cover (i.e., urban and built-up lands following the MODIS land cover products[76] with Annual International Geosphere-Biosphere Programme (IGBP) classification scheme) within the cluster. Here, we estimated the rural reference as a normalized buffer such that the area of the buffer was roughly equal to the urban cluster it surrounds, which was done using an iterative approach following Chakraborty et al.[77]. Specifically, a buffer was iteratively expanded around each urban cluster with the optimal neighborhood size chosen between 300 m to 35000 m using a step size of 300 m to generate the rural reference. For example, the area of urban cluster in Beijing was 2,739 km^2. We generated the buffer with neighborhood size of 300 m to 35000 m at 300 m intervals and calculated the area of the buffer zones respectively. We then compared the area of the different buffer zones to the area of the urban cluster and selected the buffer that most closely matched the urban area. For Beijing, the optimal neighborhood size was 6,900 m, yielding a rural reference area of 2,688 km^2. Similarly, the rural area was identified as the non-urban land cover (e.g., forests, shrublands, croplands and exclude the water) within the rural reference. Zonal statistics was conducted to calculate the spatial average value of mean daily air temperature of the urban area and rural area respectively. The UHI can be then calculated from the air temperature (Equation (1)) as:

$$UHI = Temp_{Urban} - Temp_{Rural} \tag{1}$$

$Temp_{Urban}$ indicates the mean daily air temperature spatially averaged over pixels classified as urban land covers in urban clusters while $Temp_{Rural}$ indicates the mean daily air temperature spatially averaged over non-urban land covers in the corresponding rural reference.

Trend analysis from 2003 to 2020 of monthly UHI intensity was conducted using the Seasonal Kendall test [78] in R. Kendall's τ, the slope estimate with significant t-test was used to determine the increase and decrease of UHI intensity.

Urban air pollution island intensity and trend

The difference in concentration of air pollutants, e.g., $PM_{2.5}$, between urban areas and suburban/rural areas is used to define the urban air pollution island (UPI) intensity, in analogy with the UHI. In this study, the $PM_{2.5}$ data were used as an urban air pollution indicator to calculate UPI.

$$UPI = PM_{2.5_{Urban}} - PM_{2.5_{Rural}} \tag{2}$$

$PM_{2.5_{Urban}}$ denotes the daily $PM_{2.5}$ concentration averaged over pixels classified as urban land covers in urban clusters while $PM_{2.5_{Rural}}$ denotes the daily $PM_{2.5}$ averaged over nonurban land covers in corresponding rural buffers. Similar to the trend of UHI, the trend for monthly UPI intensity from 2003 to 2020 was calculated using the Seasonal Kendall test [78].

Compound frequency, intensity and trend of UHI and UPI

The compound frequency of UHI and UPI was defined by the number of days with both existence UHI and UPI in a year as equation (3). We conducted a sensitivity analysis and compared the different thresholds to see the UHI and UPI frequency variation, as shown in Supplementary Figs. 19-21. The threshold for UHI is 0.5 $^{\circ}C$ and the threshold for UPI is 2 $\mu g/m^3$ to capture persistent but moderate urban amplification of heat and pollution exposure. While these values may appear small, they fall near the lower quartile of observed non-zero values across cities, allowing for the inclusion of frequent, low-intensity but potentially cumulative stressors.

$$UHI_{exist}^{t} = \begin{cases} 1, UHI > UHI_{threshold} \\ 0, UHI \leq UHI_{threshold} \end{cases} \tag{3}$$

$$UPI_{exist}^{t} = \begin{cases} 1, UPI > UPI_{threshold} \\ 0, UPI \leq UPI_{threshold} \end{cases} \tag{4}$$

$$Compound_{UHI\&UPI}^{Frequency} = \sum_{t=1}^{365}(UHI_{exist} \cap UPI_{exist}) \tag{5}$$

Where the UHI_{exist}^{t} denotes the daily existence of UHI, while the UPI_{exist}^{t} denotes the daily existence of UPI. t represents the day of year. The compound frequency of UHI and UPI, $Compound_{UHI\&UPI}^{Frequency}$ is the accumulated days of the co-occur of UHI and UPI within a year. The trend of yearly frequency of compound UHI and UPI from 2003 to 2020 is calculated using the Kendall test.

A compound UHI and UPI intensity index (CUHPI) was proposed to determine the compound intensity of UHI and UPI. The CUHPI was calculated using the root mean square (RMS) of the normalized UHI and UPI intensity as in equation (6). The RMS method was selected because it equally weights both components, preserves their relative magnitudes, and emphasizes higher values. This approach allows us to combine the two indicators measuring in different units into a single, dimensionless index for comparative analysis.

$$CUHPI = \sqrt{\frac{UHI_{Norm}^2 + UPI_{Norm}^2}{2}} \tag{6}$$

Where UHI_{Norm} denotes the normalized UHI intensity and the UPI_{Norm} denotes the normalized UPI intensity.

Urban heat exposure, PM$_{2.5}$ exposure and compound exposure to heat and air pollution

The urban heat exposure can be represented as the number of people with the days of high temperature in a year (people*days/year[1]) within the urban area. In this study, we assumed a daily maximum temperature higher than 35 $^{\circ}C$[79] as extreme heat. In IPCC reports, daily maximum temperature higher than 35 °C can be defined as a heat extreme[80], which is widely associated with increased heat-related mortality in epidemiological studies[81,82].

$$Exposure_{ij} = Pop_{ij} \times Days_{ij} \tag{7}$$

Where $Exposure_{ij}$ indicates the population exposure to extreme heat at grid (i, j) for one year, where the analysis scale is 1km in this study. Pop_{ij} indicates the population number of the grid (i, j) and $Days_{ij}$ indicates the number of days in a year that the temperature is higher than 35 $^{\circ}C$. We also compared the results of using locally defined extreme-heat thresholds based on the 95th percentiles of the temperature distribution for comparison (Supplementary Fig. 15), which produced spatial patterns consistent with the Global South and Global North contrasts observed in the main analysis.

The urban PM$_{2.5}$ exposure can be represented as the number of people with days of high PM$_{2.5}$ concentration (people*days/years) as in (7). In this study, we assumed that a daily PM$_{2.5}$

concentration higher than 75 $\mu g/m^3$ can be an extreme $PM_{2.5}$ concentration situation that may pose a risk to human health[83,84]. The $PM_{2.5}$ exposure threshold follows the WHO-recommended short-term interim target[85], which was relatively high in this study compared to global standards, making it particularly applicable to cities or regions with high $PM_{2.5}$ concentration, such as those in China and India.

For the compound exposure to extreme heat and air pollution, the daily maximum temperature higher than 35 $^{\circ}C$ and daily $PM_{2.5}$ concentration higher than 75 $\mu g/m^3$ simultaneously are used for yearly compound exposure analysis from 2003 to 2020.

Relative risk of high temperature related mortality

The relative risk (RR) curve was used to analyze the high temperature-related health effect[41]. It assumes a Poisson model and uses the distributed lag non-linear models (DLNM)[39,86] to fit the temperature-mortality association. A two-stage time series model was used in this study to aggregate the results of different cities into a global model[40]. In the first stage, we performed a DLNM model for different cities to get the location-specific results. In the second stage, the results of different cities were aggregated using the multivariate meta-analysis.

For the DLNM model, all variables were aggregated into daily intervals for analysis. The lag was set to 1-21 days for analysis.

$$Y_t \sim Quasipoisson$$
$$Y_t = \alpha + cbTemp_t \tag{8}$$

Where Y_t is the number of deaths related to high temperature. $Temp_t$ indicates the maximum temperature of day t. cb denotes the cross-basis function. In this study, we used B-spline bases for the daily temperature. To control the confounders, natural cubic splines of time with 5 degrees of freedom was used to depict the time series trend and seasonality. The cumulative RR, referring to the overall cumulative predicted association of different lags, was used to analyze the heat-health association.

For the multivariate meta-analysis, we pooled the location-specific results from the DLNM model for further analysis. According to the availability of the mortality data, 70 cities were chosen in this study, among which there are 53 cities in Global North and 17 cities in Global South. The mean temperature and the temperature range of Global North and Global South were considered as additional meta-predictor. Random effect multivariate meta-regression was further conducted based on the location-based DLNM results considering different UHI, UPI and compound intensity/frequency of UHI and UPI levels. High levels refer to the upper quantile of the variables while the low levels refer to the lower quantile of the variables. The Wald test is used to test the significance of different effects. The R package *dlnm* and *mvmeta* were used for the DLNM and multivariate meta analysis.

Structural equation model for urbanization impact analysis

The structural equation model[42] (SEM) has been widely used in the comprehensive multivariable analyses to understand the direction and magnitude of impacts of inputs or factors on an output variable[87-89]. In this study, we used SEM to examine the direct and indirect relationships among urbanization, compound UHI and UPI patterns, environmental stressors (temperature and $PM_{2.5}$), and mortality. Specifically, multiple factors are included: urban population density, compound frequency of UHI and UPI, compound intensity of UHI and UPI, temperature, $PM_{2.5}$, NDVI, compound exposure and mortality. Each variable was aggregated into yearly and city-level observations. There are 936 observations related to mortality and 4173 observations related to exposure in this study. All the variables were standardized (z-score) prior to model fitting. For the SEM related to mortality, three major regression models are designed for the relationship:

$$y_{mortality} \sim x_{temperature} + x_{PM2.5} + x_{compound\ intensity} + x_{compound\ frequency} \tag{9}$$

$$x_{temperature} \sim x_{population} + x_{UHI} + x_{UPI} + x_{compound\ frequency} + x_{compound\ intensity} + x_{NDVI} \tag{10}$$

$$x_{PM2.5} \sim x_{temperature} + x_{population} + x_{UHI} + x_{UPI} + x_{compound\ frequency} + x_{compound\ intensity} + x_{NDVI} \tag{11}$$

Where $y_{mortality}$ denotes the high temperature-related mortality rate. $x_{temperature}$ denotes the yearly mean daily maximum temperature, $x_{PM2.5}$ denotes the yearly mean $PM_{2.5}$ concentration.

$x_{population}$ denotes the urban population density, which can be an indicator of the urbanization degree[90]. x_{NDVI} denotes the NDVI of non-urban land cover in urban areas, which can be an indicator of urban greening. x_{UHI} denotes the annual intensity of UHI and x_{UPI} denotes the annual intensity of UPI. $x_{compound\ frequency}$ denotes the annual compound frequency of UHI and UPI. $x_{compound\ intensity}$ denotes the annual average compound intensity of UHI and UPI.

Similarly, the major regression models are designed for the SEM model related to compound exposure:

$$y_{exposure} \sim x_{temperature} + x_{PM2.5} + x_{compound\ intensity} + x_{compound\ frequency} + x_{NDVI} \tag{12}$$

$$x_{temperature} \sim x_{population} + x_{UHI} + x_{UPI} + x_{compound\ frequency} + x_{compound\ intensity} + x_{NDVI} \tag{13}$$

$$x_{PM2.5} \sim x_{temperature} + x_{population} + x_{UHI} + x_{UPI} + x_{compound\ frequency} + x_{compound\ intensity} + x_{NDVI} \tag{14}$$

Specifically, $y_{exposure}$ indicated the annual exposure. Sensitivity tests were also conducted to see the results in different compound levels (Supplementary Fig. 25).

In this model, we defined the impact of temperature/compound intensity/compound frequency on mortality/exposure as the direct effect. The pathway of temperature impact on mortality/exposure mediated via $PM_{2.5}$ is defined as the indirect effect. The pathways of compound intensity/compound frequency on mortality/exposure mediated via temperature or $PM_{2.5}$ are defined as the indirect effect of compound intensity/compound frequency. The total effect is the sum of the direct effect and indirect effect. The R package *lavaan* was used for the SEM analysis. The Global South and Global North were used as the group types to evaluate the results further (Supplementary Table 3-6).

To evaluate the fitness of this model, we considered the comparative fit index (CFI), Tucker-Lewis Index (TLI), root mean square error of approximation (RMSEA), Akaike information criterion (AIC) and standardized root mean residual (SRMR) in this study (Supplementary Table 1-2). In addition, we bootstrapped for 10000 samples to generate the 95% confidential interval for the standardized solution from the R package *semhelpinghands*.

Multilevel interaction model using the linear mixed-effects regression was used to explore the absolute impact (temperature) and relative impact (compound impact of UHI and UPI) between Global North and Global South cities. The compound impact was calculated by standardizing compound intensity and frequency separately and then averaging the two standardized variables. Specifically, we modelled mortality/exposure as a function of temperature and compound impact (the composite of compound frequency and intensity), their interactions with the categorical variable distinguishing Global North and Global South regions, and additional covariates including $PM_{2.5}$ concentration, population size and NDVI.

$$Mortality \sim Temperature \times type + compound\ impact \times type + PM_{2.5} + Population + NDVI + (1|type) \tag{15}$$

$$Exposure \sim Temperature \times type + compound\ impact \times type + PM_{2.5} + Population + NDVI + (1|type) \tag{16}$$

Where type indicates the Global North or Global South, and random intercepts were included to account for between-group variability. This formulation controls for the $PM_{2.5}$, Population and NDVI, which can explore the different impact from temperature and compound impact.

A partial correlation analysis was employed to further investigate the relationships among UHI, temperature, UPI intensity, and $PM_{2.5}$ concentrations (Supplementary Fig. 17). The Pearson correlation coefficient, along with the associated p-value, was utilized to quantitatively assess the strength and significance of these correlations.

Data availability

All data that support the findings of this study are publicly available. The urban area and base map for visualization used in this study is from the Natural Earth (https://www.naturalearthdata.com/downloads/). Environmental data include daytime and nighttime air temperature data from Zhang et al.[62], NDVI from MYD09A1 v006, land cover data from MCD12Q1, human population data from LANDSCAN (https://landscan.ornl.gov/), which can be accessed on the Google Earth Engine. Daily $PM_{2.5}$ data is from Wei et al.[38] Mortality data is from the Institute for Health Metrics and Evaluation (IHME) database (https://vizhub.healthdata.org/gbd-results/).

Code availability

The codes are available upon request.

Acknowledgements

This study was jointly supported by the National Natural Science Foundation of China (W2412136, U25A20802); the Research Grants Council (RGC) of Hong Kong, China (HKU17613022); the Croucher Foundation (CAS22902/CAS22HU01), Hong Kong, China; The Hui Oi-Chow Trust Fund, Hong Kong, China; and the Seed Fund of The University of Hong Kong, Hong Kong, China. T.C.'s contribution was supported by the U.S. Department of Energy (DOE), Office of Science, Biological and Environmental Research program through the Early Career Research Program. Pacific Northwest National Laboratory is operated for DOE by Battelle Memorial Institute under contract DE-AC05-76RL01830. Jing Wei's contribution was supported by the Fundamental and Interdisciplinary Disciplines Breakthrough Plan of the Ministry of Education of China (JYB2025XDXM906), and National Key Technology and Development Program of Corps (2025AA001).

Reference

1 Tuholske, C. *et al.* Global urban population exposure to extreme heat. *Proceedings of the National Academy of Sciences* **118**, e2024792118 (2021).
2 Xu, R. *et al.* Global population exposure to landscape fire air pollution from 2000 to 2019. *Nature* **621**, 521–529 (2023).
3 Lüthi, S. *et al.* Rapid increase in the risk of heat-related mortality. *Nature communications* **14**, 4894 (2023).
4 Hu, J. *et al.* Spatial patterns and temporal variations of footprint and intensity of surface urban heat island in 141 China cities. *Sustainable Cities and Society* **77**, 103585 (2022).
5 Niu, L., Zhang, Z., Liang, Y. & van Vliet, J. Spatiotemporal patterns and drivers of the urban air pollution island effect for 2273 cities in China. *Environment International* **184**, 108455 (2024).
6 Ritchie, H. & Roser, M. Urbanization. *Our world in data* (2018).
7 Nations, U. *2018 Revision of World Urbanization Prospects*, <https://www.un.org/en/desa/2018-revision-world-urbanization-prospects#:~:text=Today%2C%2055%25%20of%20the%20world's,increase%20to%2068%25%20by%202050.> (2018).
8 Chen, Z.-Y. *et al.* Trends in population exposure to compound extreme-risk temperature and air pollution across 35 European countries: a modelling study. *The Lancet Planetary Health* (2025).

9 Odeh, L. E. A comparative analysis of global north and global south economies. *Journal of Sustainable Development in Africa* **12**, 338–348 (2010).

10 Wang, Z.-H. Compound environmental impact of urban mitigation strategies: Co-benefits, trade-offs, and unintended consequence. *Sustainable Cities and Society* **75**, 103284 (2021).

11 Zeighami, A., Kern, J., Yates, A. J., Weber, P. & Bruno, A. A. US West Coast droughts and heat waves exacerbate pollution inequality and can evade emission control policies. *Nature Communications* **14**, 1415 (2023).

12 Chakraborty, T., Venter, Z., Qian, Y. & Lee, X. Lower urban humidity moderates outdoor heat stress. *Agu Advances* **3**, e2022AV000729 (2022).

13 Kinney, P. L. Climate change, air quality, and human health. *American journal of preventive medicine* **35**, 459–467 (2008).

14 Khraishah, H. *et al.* Climate change and cardiovascular disease: implications for global health. *Nature Reviews Cardiology* **19**, 798–812 (2022).

15 Wang, J. *et al.* Anthropogenic emissions and urbanization increase risk of compound hot extremes in cities. *Nature Climate Change* **11**, 1084–1089 (2021).

16 De Sario, M., Katsouyanni, K. & Michelozzi, P. Climate change, extreme weather events, air pollution and respiratory health in Europe. *European Respiratory Journal* **42**, 826–843 (2013).

17 Xiao, X. *et al.* Evidence of interactive effects of late-pregnancy exposure to air pollution and extreme temperature on preterm birth in China: a nationwide study. *Environmental Research Letters* **18**, 094017 (2023).

18 Rahman, M. M. *et al.* The effects of coexposure to extremes of heat and particulate air pollution on mortality in California: implications for climate change. *American Journal of Respiratory and Critical Care Medicine* **206**, 1117–1127 (2022).

19 Ballester, J. *et al.* Heat-related mortality in Europe during the summer of 2022. *Nature medicine* **29**, 1857–1866 (2023).

20 Chakraborty, T., Newman, A. J., Qian, Y., Hsu, A. & Sheriff, G. Residential segregation and outdoor urban moist heat stress disparities in the United States. *One Earth* **6**, 738–750 (2023).

21 Chambliss, S. E. *et al.* Local-and regional-scale racial and ethnic disparities in air pollution determined by long-term mobile monitoring. *Proceedings of the National Academy of Sciences* **118**, e2109249118 (2021).

22 Ahn, Y. Disparities of compound exposure of particulate matter (PM2. 5) and heat index using citywide monitoring networks. *Sustainable Cities and Society* **113**, 105626 (2024).

23 Ulpiani, G. On the linkage between urban heat island and urban pollution island: Three-decade literature review towards a conceptual framework. *Science of the total environment* **751**, 141727 (2021).

24 Sarangi, C. *et al.* Urbanization amplifies nighttime heat stress on warmer days over the US. *Geophysical Research Letters* **48**, e2021GL095678 (2021).

25 Ho, J. Y. *et al.* Urban heat island effect-related mortality under extreme heat and non-extreme heat scenarios: A 2010–2019 case study in Hong Kong. *Science of The Total Environment* **858**, 159791 (2023).

26 He, J. *et al.* Impact of the urban heat island on heat-related mortality in the Tokyo Metropolitan Area, Japan. *Environmental Research: Health* **3**, 015003 (2024).

27 Wang, S. *et al.* Dual impact of global urban overheating on mortality. *Nature Climate Change*, 1–8 (2025).

28 Lu, X. *et al.* Analysis of the adverse health effects of PM2. 5 from 2001 to 2017 in China and the role of urbanization in aggravating the health burden. *Science of the Total Environment* **652**, 683–695 (2019).
29 Kasimov, N. *et al.* Urban heat and pollution island in the Moscow megacity: Urban environmental compartments and their interactions. *Urban Climate* **55**, 101972 (2024).
30 Li, Y. *et al.* A systematic review of studies involving canopy layer urban heat island: Monitoring and associated factors. *Ecological Indicators* **158**, 111424 (2024).
31 Li, H. *et al.* Interaction between urban heat island and urban pollution island during summer in Berlin. *Science of the total environment* **636**, 818–828 (2018).
32 Kalisa, E., Fadlallah, S., Amani, M., Nahayo, L. & Habiyaremye, G. Temperature and air pollution relationship during heatwaves in Birmingham, UK. *Sustainable cities and society* **43**, 111–120 (2018).
33 De Ridder, K., Lauwaet, D. & Maiheu, B. UrbClim–A fast urban boundary layer climate model. *Urban Climate* **12**, 21–48 (2015).
34 Chakraborty, T. & Lee, X. A simplified urban-extent algorithm to characterize surface urban heat islands on a global scale and examine vegetation control on their spatiotemporal variability. *International Journal of Applied Earth Observation and Geoinformation* **74**, 269–280 (2019).
35 Li, K. & Gao, S. Global patterns and drivers of summertime surface urban heat island cohesion. *Sustainable Cities and Society*, 106470 (2025).
36 PAHO, W. Protecting health from climate change: vulnerability and adaptation assessment. *Geneva: World health Organization* (2012).
37 BELIS, C. *et al.* Urban PM2. 5 Atlas. Air Quality in Cities of Countries involved in the EU Enlargement policy.
38 Wei, J. *et al.* First close insight into global daily gapless 1 km PM2. 5 pollution, variability, and health impact. *Nature communications* **14**, 8349 (2023).
39 Gasparrini, A., Armstrong, B. & Kenward, M. G. Distributed lag non‐linear models. *Statistics in medicine* **29**, 2224‐2234 (2010).
40 Gasparrini, A. & Armstrong, B. Reducing and meta-analysing estimates from distributed lag non-linear models. *BMC medical research methodology* **13**, 1–10 (2013).
41 Gasparrini, A. *et al.* Mortality risk attributable to high and low ambient temperature: a multicountry observational study. *The lancet* **386**, 369–375 (2015).
42 Rosseel, Y. lavaan: An R package for structural equation modeling. *Journal of statistical software* **48**, 1–36 (2012).
43 Xu, F. *et al.* The challenge of population aging for mitigating deaths from PM2. 5 air pollution in China. *Nature Communications* **14**, 5222 (2023).
44 Romanello, M. *et al.* The 2021 report of the Lancet Countdown on health and climate change: code red for a healthy future. *The Lancet* **398**, 1619–1662 (2021).
45 Falchetta, G., De Cian, E., Sue Wing, I. & Carr, D. Global projections of heat exposure of older adults. *Nature Communications* **15**, 3678 (2024).
46 Liang, F. *et al.* The 17-y spatiotemporal trend of PM2. 5 and its mortality burden in China. *Proceedings of the National Academy of Sciences* **117**, 25601–25608 (2020).
47 Kaur, R. & Pandey, P. Air pollution, climate change, and human health in Indian cities: a brief review. *Frontiers in sustainable cities* **3**, 705131 (2021).

48 Venter, Z. S., Aunan, K., Chowdhury, S. & Lelieveld, J. COVID-19 lockdowns cause global air pollution declines. *Proceedings of the national academy of sciences* **117**, 18984–18990 (2020).

49 Le Quéré, C. *et al.* Temporary reduction in daily global CO2 emissions during the COVID-19 forced confinement. *Nature climate change* **10**, 647–653 (2020).

50 Wu, S., Chen, B., Webster, C., Xu, B. & Gong, P. Improved human greenspace exposure equality during 21st century urbanization. *Nature Communications* **14**, 6460 (2023).

51 Yang, Y. *et al.* Evapotranspiration on a greening Earth. *Nature Reviews Earth & Environment* **4**, 626–641 (2023).

52 Li, Y. *et al.* Green spaces provide substantial but unequal urban cooling globally. *Nature Communications* **15**, 7108 (2024).

53 Marcotullio, P. J., Keßler, C., Quintero Gonzalez, R. & Schmeltz, M. Urban growth and heat in tropical climates. *Frontiers in Ecology and Evolution* **9**, 616626 (2021).

54 Martilli, A., Krayenhoff, E. S. & Nazarian, N. Is the Urban Heat Island intensity relevant for heat mitigation studies? *Urban Climate* **31**, 100541 (2020).

55 Shaposhnikov, D. *et al.* Mortality related to air pollution with the moscow heat wave and wildfire of 2010. *Epidemiology* **25**, 359–364 (2014). https://doi.org/10.1097/EDE.0000000000000090

56 Wang, M. *et al.* The difference in the boundary layer height between urban and suburban areas in Beijing and its implications for air pollution. *Atmospheric Environment* **260**, 118552 (2021).

57 Scott, A. A., Waugh, D. W. & Zaitchik, B. F. Reduced Urban Heat Island intensity under warmer conditions. *Environmental Research Letters* **13**, 064003 (2018).

58 Kephart, J. L. *et al.* City-level impact of extreme temperatures and mortality in Latin America. *Nature medicine* **28**, 1700–1705 (2022).

59 Chakraborty, T. & Qian, Y. Urbanization exacerbates continental-to regional-scale warming. *One Earth* (2024).

60 Qiu, M. *et al.* Wildfire smoke exposure and mortality burden in the US under future climate change. (2024).

61 Chen, K. *et al.* Impact of population aging on future temperature-related mortality at different global warming levels. *Nature communications* **15**, 1796 (2024).

62 Zhang, T. *et al.* A global dataset of daily maximum and minimum near-surface air temperature at 1 km resolution over land (2003–2020). *Earth System Science Data* **14**, 5637–5649 (2022).

63 Briegel, F., Pinto, J. G. & Christen, A. Is satellite land surface temperature an appropriate proxy for intra-urban variability of daytime heat stress? *Remote Sensing of Environment* **331**, 115045 (2025).

64 Yang, G. *et al.* PM2. 5 influence on urban heat island (UHI) effect in Beijing and the possible mechanisms. *Journal of Geophysical Research: Atmospheres* **126**, e2021JD035227 (2021).

65 Martilli, A. An idealized study of city structure, urban climate, energy consumption, and air quality. *Urban Climate* **10**, 430–446 (2014).

66 Pappenberger, F. *et al.* Global forecasting of thermal health hazards: the skill of probabilistic predictions of the Universal Thermal Climate Index (UTCI). *International journal of biometeorology* **59**, 311–323 (2015).

67 Schneider, A., Friedl, M. A., McIver, D. K. & Woodcock, C. E. Mapping urban areas by fusing multiple sources of coarse resolution remotely sensed data. *Photogrammetric Engineering & Remote Sensing* **69**, 1377–1386 (2003).

68 Affairs, U. N. D. o. E. a. S. *World Urbanization Prospects 2018*, <https://population.un.org/wup/Download/> (2018).

69 Castells‐Quintana, D., Royuela, V. & Veneri, P. Inequality and city size: An analysis for OECD functional urban areas. *Papers in Regional Science* **99**, 1045–1064 (2020).

70 Rose, A., McKee, J., Sims, K., Bright, E., Reith, A., & Urban, M. (2021).

71 Zhang, T., Zhou, Y., Wang, L., Zhao, K. & Zhu, Z. Estimating 1 km gridded daily air temperature using a spatially varying coefficient model with sign preservation. *Remote Sensing of Environment* **277**, 113072 (2022).

72 Vermote, E. MOD09A1 MODIS/terra surface reflectance 8-day L3 global 500m SIN grid V006. *NASA EOSDIS Land Processes DAAC* **10** (2015).

73 Sulla-Menashe, D. & Friedl, M. A. User guide to collection 6 MODIS land cover (MCD12Q1 and MCD12C1) product. *Usgs: Reston, Va, Usa* **1**, 18 (2018).

74 Gorelick, N. *et al.* Google Earth Engine: Planetary-scale geospatial analysis for everyone. *Remote sensing of Environment* **202**, 18–27 (2017).

75 Murray, C. J. *et al.* Global burden of 87 risk factors in 204 countries and territories, 1990–2019: a systematic analysis for the Global Burden of Disease Study 2019. *The lancet* **396**, 1223–1249 (2020).

76 Friedl, M. & Sulla-Menashe, D. MODIS/Terra+ Aqua land cover type yearly L3 Global 0.05 Deg CMG V061. *NASA EOSDIS Land Processes Distributed Active Archive Center (DAAC) data set*, MCD12C11. 061 (2022).

77 Chakraborty, T., Sarangi, C. & Lee, X. Reduction in human activity can enhance the urban heat island: Insights from the COVID-19 lockdown. *Environmental Research Letters* **16**, 054060 (2021).

78 Libiseller, C. & Grimvall, A. Performance of partial Mann–Kendall tests for trend detection in the presence of covariates. *Environmetrics: The official journal of the International Environmetrics Society* **13**, 71–84 (2002).

79 Jones, B. *et al.* Future population exposure to US heat extremes. *Nature Climate Change* **5**, 652–655 (2015).

80 Seneviratne, S. I. *et al.* Weather and climate extreme events in a changing climate. *Climate change 2021: The physical science basis: Working group I contribution to the sixth assessment report of the intergovernmental panel on climate change*, 1513–1766 (2021).

81 Günsche, S. *et al.* Mortality, morbidity and healthcare costs of short-term high temperatures and heatwaves exposure in older populations: a global systematic review and meta-analysis. *Environment International*, 110129 (2026).

82 Pan, R. *et al.* The impact of heat waves on the mortality of Chinese population: A systematic review and meta-analysis. *Medicine* **102**, e33345 (2023).

83 Carvalho, H. New WHO global air quality guidelines: more pressure on nations to reduce air pollution levels. *The Lancet Planetary Health* **5**, e760–e761 (2021).

84 (WHO), W. H. O. *WHO Air Quality Guidelines*, <https://www.c40knowledgehub.org/s/article/WHO-Air-Quality-Guidelines?language=en_US#:~:text=By%20reducing%20air%20pollution%20levels,3%20%2D%204%20days%20per%20year> (2021).

85 Organization, W. H. *WHO global air quality guidelines: particulate matter (PM2. 5 and PM10), ozone, nitrogen dioxide, sulfur dioxide and carbon monoxide*. (World Health Organization, 2021).

86 Gasparrini, A. Distributed lag linear and non-linear models in R: the package dlnm. *Journal of statistical software* **43**, 1 (2011).

87 Huang, G. & Cadenasso, M. People, landscape, and urban heat island: dynamics among neighborhood social conditions, land cover and surface temperatures. *Landscape ecology* **31**, 2507–2515 (2016).

88 Liang, Z. *et al.* The mediating effect of air pollution in the impacts of urban form on nighttime urban heat island intensity. *Sustainable Cities and Society* **74**, 102985 (2021).

89 Zhang, L., Yang, X., Fan, Y. & Zhang, J. Utilizing the theory of planned behavior to predict willingness to pay for urban heat island effect mitigation. *Building and Environment* **204**, 108136 (2021).

90 Michele, M. *et al.* Applying the Degree of Urbanisation Method to National Population and Housing Census with GHSL Tools. (2021).

Fig. 1 | Compound frequency and intensity of UHI and UPI in 327 cities from 2003 to 2020. a, Annual mean compound frequency of UHI and UPI (number of days/year) for global cities from 2003 to 2020. **b**, Summary of compound frequency of UHI and UPI of Global North and Global South cities from 2003 to 2020. **c**, The mean compound intensity of UHI and UPI for global cities from 2003 to 2020. **d**, Summary of compound intensity of UHI and UPI of Global North and Global South cities from 2003 to 2020. **e**, The top 20 cities with the highest compound frequency of UHI and UPI and their associated compound intensity of UHI and UPI. **f**, Time series compound frequency of UHI and UPI for Global South and Global North cities from 2003 to 2020. **g**, Time series compound intensity of UHI and UPI for Global South and Global North cities from 2003 to 2020. Pairwise T-tests were conducted to determine the significance level between the Global North and South cities. '***' indicates significant differences at the 0.001 levels.

Fig. 2 | Compound exposure to extreme heat and air pollution in global cities. a, Averaged compound exposure to heat and air pollution **(**$PM_{2.5}$) from 2003 to 2020, the threshold of daily extreme heat was 35 degrees and the threshold of daily extreme $PM_{2.5}$ was 75 ug/m^3. **b**, Averaged exposure (million person-days/year) to heat, $PM_{2.5}$ and compound exposure of cities in Global North and Global South from 2003 to 2020. **c**, Time series annual compound exposure (million person-days/year) to extreme heat and air pollution of cities from 2003 to 2020. **d**, Time series annual exposure (million person-days/year) to extreme heat and air pollution of cities from 2003 to 2020. **e**, Averaged exposure (million person-days/year) to heat, $PM_{2.5}$, and compound exposure of cities with UHI, UPI, both UHI & UPI and non UHI & UPI (NA) from 2003 to 2020.

Fig. 3 | Cumulative relative risk (RR) of cities in high and low compound intensity and frequency of UHI and UPI levels and different groups. a, RR in high and low compound frequency of UHI and UPI levels. **b**, RR in high and low compound intensity of UHI and UPI levels. **c**, RR of cities globally, in Global North and in Global South with different compound frequency of UHI and UPI, and compound intensity of UHI and UPI levels. **d**, RR of different sex groups in global cities with different compound frequency of UHI and UPI, and compound intensity of UHI and UPI levels. **e**, RR of different age groups in global cities with different compound frequency of UHI and UPI, and compound intensity of UHI and UPI levels. The vertical lines denote the percentile of minimum mortality temperature (dotted) and the 90th and 99th percentiles of the temperature distribution (dashed).

Fig. 4 | The structural equation model of the correlation of annual urban population, compound frequency of UHI and UPI, compound intensity of UHI and UPI, $PM_{2.5}$, temperature, greening and exposure/mortality at city level from 2003 to 2019. **a**, Correlation among the urban population, compound frequency of UHI and UPI, compound intensity of UHI and UPI, temperature, $PM_{2.5}$, greening and exposure (N=4173) using structural equation model (SEM). **b**, Multilevel regression between temperature and compound exposure. **c**, Multilevel regression between compound impact (compound intensity and compound frequency) and compound exposure. **d**, Correlation among the urban population, compound frequency of UHI and UPI, compound intensity of UHI and UPI, temperature, $PM_{2.5}$, greening and mortality (N=936) using the SEM. **e**, Multilevel regression between temperature and mortality. **f**, Multilevel regression between compound impact (compound intensity and compound frequency) and mortality. Freq indicates the compound frequency of UHI and UPI and Intens indicates the compound intensity of UHI and UPI. Urbanization is indicated by the mean urban population density within the urban areas. Urban greening is indicated by mean NDVI within the urban areas. The red arrows show the positive effect while the blue arrows show the negative effect with significant level $P<0.01$. The dash grey arrows indicate the insignificant effect. The values on the arrow indicate standardized coefficients and statistical significances of the endogenous variables.

Fig. 5 | Direct, indirect and total effects of temperature and compound patterns of UHI and UPI on mortality rate/exposure in Global South and Global North cities. a. The direct, indirect and total effects of temperature. b, The direct, indirect, and total effects of compound frequency of UHI and UPI, and compound intensity of UHI and UPI.

Author Contributions

Y.L. wrote the main manuscript. H.Z. and Y.Z. jointly supervised the research and edited the manuscript. T.C., S.W., Y.C. and P.G. edited the manuscript. J.W. provided dataset for this research. All authors reviewed the manuscript.

Ethics declarations

Competing interests

The authors declare no competing financial or non-financial interests.